The *Shewanella oneidensis* MR-1 fluxome under various oxygen conditions

Yinjie J. Tang[1,3,*], Judy S. Hwang[1,2,*], David E. Wemmer[1,2,4],

and Jay D. Keasling[1,3,5,#]

[1]Physical Biosciences Division, Lawrence Berkeley National Laboratory, Berkeley, CA 94720

[2]Biophysics Graduate Group, Departments of [3]Chemical Engineering, [4]Chemistry, and

[5]Bioengineering, University of California, Berkeley, CA 94720

* These authors contributed equally to the work.

Corresponding author:

Berkeley Center for Synthetic Biology

University of California

Berkeley, CA 94720

Phone: (510) 642-4862; Fax: (510) 495-2630; Email: Keasling@berkeley.edu

Abstract

The central metabolic fluxes of *Shewanella oneidensis* MR-1 were examined under carbon-limited (aerobic) and oxygen-limited (micro-aerobic) chemostat conditions using ^{13}C labeled lactate as the sole carbon source. The carbon labeling patterns of key amino acids in biomass were probed using both GC-MS and ^{13}C-NMR. Based on the genome annotation, a metabolic pathway model was constructed to quantify the central metabolic flux distributions. The model showed that the tricarboxylic acid (TCA) cycle is the major carbon metabolism route under both conditions. The Entner-Doudoroff and pentose phosphate pathways were utilized primarily for biomass synthesis (flux below 5% of the lactate uptake rate). The anapleurotic reactions (pyruvate to malate and oxaloacetate to phospho*enol*pyruvate) and the glyoxylate shunt were active. Under carbon-limited conditions, a substantial amount (9% of the lactate uptake rate) of carbon entered the highly reversible serine metabolic pathway. Under micro-aerobic conditions fluxes through the TCA cycle decreased and acetate production increased compared to carbon-limited conditions, and flux from glyoxlate to glycine (serine-glyoxylate aminotransferase) became measurable. Although flux distributions under aerobic, micro-aerobic, and shake-flask culture conditions were different, the relative flux ratios of some central metabolic reactions did not vary significantly (in particular, between shake flask and aerobic chemostat). Hence, *S. oneidensis* central metabolism appears to be robust to environmental changes. Our study also demonstrates the merit of coupling GC-MS with ^{13}C NMR for metabolic flux analysis to reduce the use of ^{13}C labeled substrates and to obtain more accurate flux values.

Key words: micro-aerobic, isotopomer model, futile cycles, serine metabolism, flux ratio

Introduction

Shewanella oneidensis MR-1 (ATCC70050) is a Gram-negative, facultative anaerobe that was isolated from lake sediment (35). These bacteria are capable of utilizing many carbon sources, including lactate, acetate, pyruvate, and some amino acids. Moreover, they are capable of reducing a variety of electron acceptors besides oxygen, including Fe(III), Mn(IV), sulfur, nitrate, and fumarate (26). There have been extensive studies of this strain, primarily focused on its versatile respiration and its potential to engage in co-metabolic bioremediation of toxic metals (17, 18, 34, 36, 37).

Recently, the complete genome was sequenced and annotated. Furthermore, key phenotypic and molecular characteristics have been identified (13). *S. oneidensis* central carbon metabolism under both aerobic and anaerobic conditions has been investigated using enzyme assays and genome information (11, 26, 27), and there are several unusual features (26, 42). First, a serine pathway is proposed to be active under anaerobiosis in *S. oneidensis* due to the detection of high levels of hydroxypyruvate reductase, which is the key enzyme involved in serine metabolism. Second, *S. oneidensis* shares some metabolic features with non-fermentative Pseudomonads, such as utilizing the Entner-Doudoroff (ED) pathway instead of the Embden-Meyerhof-Parnas (EMP) pathway for the oxidation of glucose. Third, because the TCA cycle might be truncated under oxygen limited conditions, the glyoxylate shunt might be present to synthesize TCA cycle intermediates. However, these features have not been rigorously verified using ^{13}C tracer experiments, and very little is known about the actual balances of intracellular metabolic fluxes under different oxygen conditions. Metabolic flux analysis is necessary to provide a detailed physiological characterization of *S. oneidensis* MR-1 and may be important

for improving its metal reduction ability through rational metabolic engineering or by stimulating metal reduction in the environment through addition of growth supplements and electron donors.

^{13}C isotopomer analysis is a powerful approach to map intracellular fluxes. By feeding a ^{13}C-labeled carbon source to the cells, the labeling pattern of primary metabolites, often the amino acids, can be measured. Based on these isotopomer data and the biochemical network of *S. oneidensis* MR-1, a metabolic pathway model can quantify the rates of intracellular reactions (16). In our study, labeling patterns of amino acids were analyzed by both nuclear magnetic resonance (NMR) spectroscopy and gas chromatography-mass spectrometry (GC-MS). The advantage of NMR is that it provides positional information about the labels in the isotopomers even though detection sensitivity is low (2). GC-MS is a more sensitive detection method and determines what fraction of a particular molecule or molecular fragment contains a specific number of labels (38). By combining GC-MS and NMR data, a complete picture of the isotopomer distribution in amino acids can be obtained. The main goal of this study was to determine the fluxes through key metabolic pathways in *S. oneidensis* MR-1 under aerobic and micro-aerobic conditions. The determination of fluxes was accomplished in three steps: 1) the cells were grown in defined medium with ^{13}C-labeled lactate as the sole carbon source; 2) the labeling patterns in key amino acids of the total protein hydrolysate were characterized using both GC-MS and NMR; and 3) a flux calculation algorithm was used to quantify the central metabolic pathways. Two sets of conditions were probed to determine the flux distribution, carbon limitation (DO>70%) and oxygen limitation (DO<10%). The results not only widen our understanding of *Shewanella* metabolism but also demonstrate a powerful approach for investigating metabolic flux analysis using both GC-MS and NMR techniques.

Material and methods

Culture conditions

S. oneidensis MR-1 was purchased from American Tissue Culture Center (ATCC 70050) and was stored at -80°C prior to use. All cultures used the modified MR-1 defined medium (31) (supplementary materials). The lactate used was either [3-^{13}C] sodium L-lactate (98%, Cambridge Isotope, USA), [1-^{13}C] sodium L-lactate (99%, Cambridge Isotope, USA), or a mixture of 10% [$^{13}C_3$] sodium L-lactate (99%, Cambridge Isotope, USA) and 90% unlabeled sodium lactate (Fisher, USA).

Fermentations were carried out in a 1-L New Brunswick Bioflo 110 fermentor. The off-gas composition was analyzed using a mass spectrometer (Thermo Onix). The inoculum was prepared in LB medium in shake flasks overnight (optical density at a wavelength of 600 nm, OD_{600}>1.5). Fermentations were started with a 1% inoculated volume for optimal growth kinetics. After three residence times in continuous mode, the amount of LB remaining would be very small (<0.05%). The reactor temperature was maintained at 30°C. The working volume in the bioreactor was kept at 500 mL, and agitation was set at 300 rpm. For the carbon-limited condition, 30 mM [3-^{13}C] L-lactate was used, and the dilution rate was set to 0.079 hr^{-1} in order to keep the DO level over 70% during continuous culture. For the oxygen-limited condition, 50 mM lactate composed of 10% [$^{13}C_3$] L-lactate and 90% unlabeled lactate was used. The dilution rate was set to 0.10 hr^{-1}, and the DO was controlled below 10% during continuous culture. In both experiments, the continuous culture was started after 15 hours of batch culture and continued for three generations. During both continuous cultures, the medium was controlled at pH ~8 and final OD_{600} is around one. ^{13}C-Labeled biomass was sampled after three generation times for biomass composition analysis and isotopomer measurements. For shake-flask

experiments, cells were grown in 10 ml of three differently labeled lactate media (shaking speed = 200rpm): [3-^{13}C] L-lactate, [1-^{13}C] L-lactate, or [$^{13}C_3$] lactate (10% [$^{13}C_3$] L-lactate with 90% unlabeled lactate). The final concentration of lactate was 30 mM. The MR-1 inoculum was prepared in labeled modified MR-1 defined medium, and 2% of the final culture volume was inoculated into the same medium in shake flasks. The biomass in shake flasks was harvested in the mid-exponential growth phase (OD_{600} ~0.5).

Analytical methods for extracellular metabolites and biomass compositions

Cell growth was monitored by measuring the OD_{600}. The harvested culture was centrifuged at 4800 × g and 4°C for 20 min and lyophilized overnight. The dried biomass was weighed and used for fatty acid quantification using fatty acid methyl ester (FAME) analysis (33) (Microbial ID, Newark, Delaware). The total protein concentration was determined by the Bradford Protein Assay (BioRad Cat#500-0006). The concentrations of lactate, acetate, pyruvate, and succinate in the medium were measured using enzyme kits (r-Biopharm, Darmstadt, German), and lactate, pyruvate, and acetate were also quantified using 1D ^{1}H presaturation NMR spectra. The relaxation delay between scans was set to 20 s, and 100 μM sodium 3-trimethylsilylpropionate (TSP) added to the sample was used as the reference compound for quantification. The reported results are the average of both enzymatic and NMR measurements.

All measurement methods for biomass constituents (protein, carbohydrates, RNA, and DNA) were taken from previously reported protocols (4, 15, 16). Total protein content was determined using the Bradford method, carbohydrate was determined by the phenol reaction, RNA was assayed through a reaction involving orcinol, and DNA was obtained through the colorimetric procedure that involves the reaction of DNA with diphenylamine in a mixture of

perchloric acid. Glucose, pure *E. coli* RNA (Ambion #7940), and deoxyribose were used as standards for the carbohydrate, RNA, and DNA measurements, respectively. Quantification of amino acids in protein was performed by the Molecular Structure Facility (University of California, Davis).

Gas chromatography-Mass spectrometry

Before measuring amino acid labeling patterns in cellular protein, a 10 mL culture was harvested and centrifuged down at 8000 g. The cell pellets were washed once with 0.9% NaCl; then suspended in 1 ml of sterile nanopure water and sonicate using the microtip for 3 min with a 3 sec. on/1 sec. off cycle. The proteins from the resulting lysate were precipitated using trichloroacetic acid and washed with cold acetone two times; then hydrolyzed in 6 M HCl at 100°C for 24 hours. GC-MS was carried out using a gas chromatograph (DB5 column, HP6890 series, Agilent Inc, USA) equipped with a mass spectrometer (5973 Network, Agilent Inc, USA). GC-MS samples were prepared in 100 µl of tetrahydrofuran (THF) and 100 µl of N-(tert-butyldimethylsilyl)-N-methyl-trifluoroacetamide (Sigma-Aldrich, USA). All samples were derivatized in a water bath at 65-80°C for 1 hour. Two types of positively charged species were clearly observed by MS in this study: unfragmented molecules, $[M-57]^+$, and fragmented molecules that had lost one carboxyl group, $[M-159]^+$. M is the total molecular mass of the derivatized hydrolysate component, and 57 indicates the loss of 57 mass units, e.g. a tert-butyl group. For amino acids that contain two carboxyl groups, the loss of the α-carboxyl group is strongly favored because the amine group on the β-carbon allows the formation of an entropically stable fragment (6, 12). The natural abundance of isotopes, including ^{13}C (1.13%), ^{18}O (0.20%), ^{29}Si (4.70%) and ^{30}Si (3.09%) (Si occurs in amino acids derivatized for gas chromatography separation), change the mass isotopomer spectrum. These changes were

corrected using a published algorithm before using the data for calculating the label distribution (14).

^{13}C NMR sample preparation and analysis

An aliquot (50 ml) of culture was harvested by centrifuging at 5000 × g for 20 min at 4°C. The cell pellet was washed twice with 20 mM NaH_2PO_4 (in D_2O) (pH 7) buffer. Washed pellets were resuspended in the same buffer, and the cells were disrupted by sonication. Cells were sonicated for 4-5 times with 15-20 seconds each time at sonication power 3 on Misonix sonicator 300 (Misonix Inc., USA). Cell debris was removed by centrifugation at 11,250 × g for 30 minutes at 4°C. Cellular protein in the supernatant was then hydrolyzed in 6 M HCl by incubation at 95-100°C for 24 hours. The hydrolysate was filtered through a 0.22-μm-pore-size filter and lyophilized. The dried material was dissolved in 700 μl of 20 mM deuterium chloride (DCl) in D_2O, filtered through a 0.22-μm-pore-size filter, and used for the NMR measurements.

Proton-detected 2D ^{13}C-^{1}H heteronuclear single-quantum COSY (HSQC-COSY) spectra were collected with the pulse sequence and parameters as described in (5). The spectra were recorded at a ^{1}H frequency of 600 MHz on a Bruker DRX 600 spectrometer and analyzed with the software NMRPipe and NMRDraw (5). For each sample, two spectra were taken: one for the aliphatic resonances with the ^{13}C carrier set to 43 ppm, and the other spectrum for the aromatic resonances with the ^{13}C carrier set to 125 ppm. The data sizes were 3,500 × 1,024 complex points. The acquisition times were t_{1max} = 686 msec and t_{2max} = 128 msec. The relaxation delay between scans was set to 2.2 - 2.3 s, and the spectra were collected at 25°C for all 2D NMR experiments. The relative distribution of the isotopomers was determined from the intensities of the individual multiplet components in ^{13}C-^{13}C scalar coupled multiplets (30).

Algorithm for flux calculation and isotopomer modeling

Central biochemical pathways for *S. oneidensis* MR-1 were selected based on the internet-accessible genome data base MicrobesOnline (1). The complete list of key reactions in the model is given in Supplementary Material, and the reaction network is shown in Figure 1. The pathway map includes the tricarboxylic acid (TCA) cycle (including the glyoxylate shunt), C_1 metabolism, the Entner-Doudoroff (ED) pathway, and the pentose phosphate (PP) pathway. The shaded boxes represent the biomass pool containing key amino acids for which the isotopomer distributions were measured by GC-MS and NMR. There are 36 free fluxes to be determined in the pathway map. The extracellular fluxes, v1 and v6, were directly measured using enzymatic methods. An isotopomer solution algorithm was developed using MATLAB 6.0 (The Mathworks, Massachusetts, U.S.A.). To search for a global solution, an iterative procedure, which consisted of the following steps, was used. 1) A set of initial guesses for all fluxes was input to the solution algorithm. The speed of converging to a global solution depends on the guess of the initial value. The starting guess of independent fluxes was coarsely based on MR-1 biomass composition or previous reported fluxes for the well-known microorganism, *Escherichia coli*. After each round of iteration, a set of improved guessed fluxes was found and then used as a new search point. The complete fluxes in the pathway map were solved using the reaction stoichiometric matrix (29). 2) Concepts of atom mapping matrices (AMM) and isotopomer mapping matrices (IMM) were used in an iterative scheme to calculate the steady-state isotopomer distributions in the intracellular metabolite pools, and these were transformed to MS and NMR data (24, 25). The simulated MS and NMR data for isotopomer distributions of proteinogenic amino acids were compared to the experimental results. 3) For each search point, the local optimal solution was found using Nelder-Mead method (via the fminsearch function in

MATLAB). 4) A simulated annealing strategy was used to obtain an optimal global solution. First, an optimal local solution was perturbed by taking a finite amplitude step away from it, and then steps 1-4 were repeated to see if a better solution could be obtained. The global search stopped when the objective function could not be further minimized (20). The objective function is defined as:

$$\varepsilon(v_n) = \sum_{i=1}^{a}\left(\frac{M_{i,m} - M_{i,c}(v_n)}{\delta_i}\right)^2 + \sum_{j=1}^{b}\left(\frac{N_{j,m} - N_{j,c}(v_n)}{\delta_j^{'}}\right)^2 \quad (1)$$

where ν_n are the unknown fluxes to be optimized in the program, $M_{i,m}$ are the measured MS data, and $M_{i,c}$ are the corresponding model simulated values. $N_{i,m}$ are the measured NMR data, and $N_{i,c}$ are the corresponding model simulated values. δ and δ' are the experimental errors for measured MS and NMR data, respectively. To save computational time, biomass fluxes were constrained based on the uncertainty of the measurement. The confidence intervals of the calculated fluxes can be estimated by Monte Carlo methods (20): 1) the measured data were perturbed randomly within measurement noise; 2) the optimization routine described above was used to estimate the new flux distribution after each perturbation; 3) after testing over 100 simulated measured data sets, the error bounds on the flux distributions resulting from errors in all measurements were obtained.

All reactions could be potentially reversible and make the system highly underdetermined (29). Several reactions (v4, v5, v11, v8 v12, and v21) were considered to be reversible because they have the most significant impact on the isotopomer distribution (2, 43). The reversible reactions are characterized by their net flux, v_i, and their exchange flux, v_i^{exch}. The net flux is defined as the difference between forward and backward fluxes. The exchange flux, v_i^{exch}, is the

smaller of the forward and backward fluxes. Equation 2 rescales v_i^{exch} (possible value range [0, ∞]) to exchange coefficients, $exch_i$, which has a finite range [0, 1] (39):

$$v_i^{exch} = \beta \frac{exch_i}{1 - exch_i} \quad (2)$$

where β is a constant of the order of magnitude of v_i. In our study, a value of one was assigned to β. Exchange coefficients are limited to values between 0 and 0.95 in order to improve the speed of convergence.

Sensitivity test of isotopomer model

The flux calculation is based on tracing the path of ^{13}C from labeled carbon substrate to metabolites in the pathway network. Singly-labeled or fully-labeled ^{13}C substrate (often 10-20%) can be used for tracer experiments in flux analysis (8). Although the labeling pattern of substrate should not affect the actual flux distributions, it may affect the sensitivity of isotope data to model calculations (2, 40). Some studies have shown that the ED and PP pathways are particularly well resolved using singly-labeled carbon substrate, whereas the fully-labeled carbon substrate is ideal for reactions in the TCA cycle because information from ^{13}C-^{13}C connectivity can be obtained (9). Other studies have shown that the use of a mixed labeling pattern (containing certain percentages of unlabeled, fully-labeled, and doubly-labeled substrate) may be the most useful to ascertain metabolic fluxes (2). However, most studies on sensitivity of isotopomer distributions have used glucose as the carbon source and focused on GC-MS as the only measurement technique. To avoid potential bias in calculated fluxes, our study utilized two different labeling strategies: 10% fully-labeled lactate for the oxygen-limited chemostat and 98% singly-labeled lactate for the carbon-limited chemostat. To minimize the cost of labeled lactate

for fermentations, these two types of labeled lactate medium were also used in shake-flask cultures to provide an additional comparison for sensitivity analysis.

After obtaining global solutions for flux distributions of cells grown under different culture conditions, a sensitivity test is necessary to check the reliability of the model results and to estimate the confidence interval of the calculated fluxes. The sensitivity coefficient, which reflects the sensitivity of mass distribution upon changes in fluxes and exchange coefficients, is defined as:

$$S_{i,j} = \frac{\partial I_i}{\partial v_j} \approx \frac{I_i^{'} - I_i}{v_j^{'} - v_j} \quad (3)$$

where I_i is the isotopomer data for amino acid (i) and v_j is the flux or exchange coefficient (j) (2). Since the analytical expression is difficult to derive, an approximation has to be made. After the global solution is found with the best fitted isotopomer data, I_i, the optimized flux distribution, v_j, is then perturbed with a small change in its independent fluxes and exchange coefficients. The resulting new flux distribution ($v_j^{'}$) predicts a new set of isotopomer data ($I_i^{'}$), and Equation 3 can be applied to estimate the sensitivity of the model.

Results

Aerobic chemostat and shake flask cultivations

Continuous cultivation was performed under two conditions: carbon limitation (30 mM lactate, DO>70%) and oxygen limitation (50 mM lactate, DO<10%). Cell growth, lactate consumption, and acetate production were measured during the cultivation (Figure 2). During the batch phases of both conditions, some of the lactate was converted to acetate. Under the carbon-limited condition with a low growth rate (D=0.079 hr^{-1}), neither lactate nor acetate was detected in the effluent of the continuous culture; while under the oxygen-limited condition with

a higher growth rate (D=0.10 hr^{-1}), 17.5 mM acetate was detected in the effluent of the continuous culture. The CO_2 concentration in the off-gas remained constant after two generations. A similar final OD_{600} and biomass concentration were the basis for our comparison between these two chemostat cultures (Table 1). In parallel with the continuous culture, *S. oneidensis* MR-1 was grown in shake flasks with labeled lactate. The profiles of growth, lactate consumption, and acetate production were similar to those of the batch phase of chemostat cultures (data not shown). The observed doubling time in defined medium was approximately 4 hrs, which was equivalent to a growth rate of 0.17 hr^{-1}. The results also reflect the growth kinetics of *S. oneidensis* MR-1: a high growth rate and low dissolved oxygen level enhanced acetate production under aerobic conditions (32).

Biomass composition analysis

Analysis of biomass composition not only helps understand the biosynthetic kinetics, but also provides the initial guesses for some intracellular fluxes in our calculation algorithm. The biomass compositions of *S. oneidensis* MR-1 grown under both shake flasks and chemostat conditions are similar to those of *E. coli*, even though *E. coli* was grown on a different carbon source under different growth conditions (Table 2). The RNA and DNA fractions of the biomass from the shake-flask cultures were relatively similar to those observed in the chemostat cultures, whereas the fatty acid fraction of the shake-flask cultures was much less than that of the chemostat cultures. The undetermined weight fraction was probably soluble metabolites, residual salts, and bound water that was not completely removed from the biomass by lyophilization. FAME analysis showed that the fatty acid profile was dominated by even-numbered fatty acids (Supplementary Table 1). The amino acid mole fractions from cellular protein were very similar in the two chemostat cultures and the shake-flask cultures

(Supplementary Figure 1). This may indicate that even though specific proteins are different under the two conditions, the amino acid fractions in total proteins do not change under those growth conditions.

Isotopomer distribution profiles

Although NMR and MS analyses have both been used successfully in previous work, the latter was thought to be high-throughput and more sensitive (≤ 2% errors) with comparatively low cost (22). Application of GC-MS to separate the derivatized protein hydrolysate gave chromatographic peaks of 15 proteinogenic amino acids (arginine, asparagine, cysteine, glutamine, and tryptophan could not be determined). The possible alternative routes for leucine and isoleucine synthesis suggested by the MR-1 genome information are complicated, and both amino acids' MS peak $[M-57]^+$ were overlapped by other signals, so their isotopomer distributions were not considered in the model calculation. Consistent with assumed amino acid biosynthesis pathways, several amino acid pairs derived from the same precursor, such as proline and glutamate (from precursor oxoglutarate), threonine and aspartate (from precursor oxaloacetate), tyrosine and phenylalanine (from precursors phospho*enol*pyruvate and erythrose-4-phosphate), had similar isotopomer patterns from both MS and NMR measurements (29). This redundant isotopomer information could be utilized to estimate the experimental errors (8).

Flux analysis requires the pools of intracellular metabolites to be in isotopomeric steady state. Although flux analysis is best studied in physiological steady state by continuous bioreactor culture, many studies have shown that a (quasi) steady state can also be achieved during the exponential growth phase (or even at stationary phase) in batch culture (7, 23, 28). As a convenient and less expensive approach to test the reproducibility of isotopomer distribution determinations, biomass was also cultured in 10-mL shake flasks using the same medium as the

chemostat cultures. The isotopomer distributions of key amino acids from shake-flask and chemostat cultures had relatively similar profiles with less than 10% difference (fragment $[M-57]^+$ in Table 3 and fragment $[M-159]^+$ in Supplementary Table 2). There were larger differences (10-15%) in the isotopomer ratios of the mass fragments of phenylalanine between the carbon-limited chemostat and shake-flask cultures.

The ^{13}C abundance for individual carbon positions is helpful to identify reactions in the metabolic network and to provide additional constraints for the isotopomer model. In this study, the labeling patterns of the key amino acids in the hydrolysate were analyzed by 2D [^1H-^{13}C] COSY NMR. In the indirectly detected ^{13}C dimension, multiplets arise from scalar spin-spin coupling between directly linked ^{13}C carbon spins. For the α-carbon of a fractionally labeled amino acid, up to four different patterns of multiplets (isotopomers) may be observed. Based on the ratios of peak intensities, the relative populations of isotopomers can be determined (29). However, because of some overlap in multiplet peaks and signals arising only from the natural abundance ^{13}C, estimations of the isotopomer distributions were not always unique. Therefore, model calculations only considered the most reliable NMR data of nine amino acids for the isotopomer model analysis, mainly from α and β carbons (Table 4).

Flux calculation and model reliability test

The isotopomer model provided flux distributions for both chemostat cultures and shake-flask cultures. The lactate carbon flux (taken to be 100%) is split into two branches at pyruvate: one flows towards the TCA cycle and the other flows towards the PP and ED pathways (Figure 3). For the carbon-limited condition, 61% of the substrate entered the TCA cycle via acetyl-CoA condensing with oxaloacetate. For the micro-aerobic condition, the TCA cycle was weakened, as the relative carbon flux through the TCA cycle dropped to 47%; approximately 35% of the

lactate was converted into acetate. Additionally, the calculations indicate that some fluxes might be highly reversible, such as the serine metabolism route. The reversibility of the serine metabolism route could alter the mass distribution of serine and glycine significantly. Although all the reactions in the PP pathway were thought to be reversible, the total fluxes through the PP reactions were small (< 4% of the lactate uptake); thus, the reversibility could be neglected in the model in order to reduce computation time (43). Studies have shown that ^{13}C tracer experiments only give crude estimates of some exchange rates (often within one order of magnitude); thus, there is no need to consider the reversibility of every reaction (25, 41).

The reliability of model results was checked using sensitivity coefficients, which are a similar concept to the model objective function (Equation 1) (43). By making small changes to specific optimized fluxes, the resulting new fluxes predicted the changes in isotopomer distributions of specific amino acids. For example, by increasing or decreasing the pyruvate-to-malate flux, the model predicted the change in isotopomer distributions of Asp and Glu. The absolute value of the sensitivity coefficients was evaluated, and then the sum of their squares was determined (Table 5). As for 98% 3rd position labeled lactate, the model was sensitive to both GC-MS and NMR data based on the sum of the squared sensitivity coefficients (GC-MS: 0.00077 and NMR: 0.00082). On the other hand, the sum of the squared sensitivity coefficients using 10% fully-labeled lactate (GC-MS: 0.00007) was one order-of-magnitude lower than that using the singly-labeled lactate. This indicated that using GC-MS data from 10% fully-labeled lactate experiments might produce biased results. However, the model was very sensitive to NMR data when 10% labeled lactate was used. Coupling NMR analysis with GC-MS could significantly improve the resolution of model calculations when a low fraction of fully-labeled substrate is used.

In general, the predicted amino acid isotopomer distributions matched reasonably well with both experimental GC-MS and NMR data (Tables 3 and 4 and Supplementary Table 2), which indicated the accuracy of the model calculation. Besides the instrument errors (GC-MS error: 1-2% and NMR error: 4-5%), differences between modeled and measured isotopomer data could arise from other possible sources: 1) measurement errors of the extracellular fluxes, 2) background noise from the 1.13% natural abundance ^{13}C, and 3) simplification of the model by neglecting the reversibility of less influential pathways. All the above sources complicate the error estimation. An in-depth analysis of the discrepancy between the model fitting and the experimental data is beyond the scope of this paper.

Discussion

The TCA cycle and serine oxidation pathway (energy production pathways)

The TCA cycle was the main carbon metabolism route (fluxes >60% of lactate uptake) and the flux toward a reversible serine oxidation pathway (PEP to serine to glycine to C1) was almost 10% of lactate uptake under carbon-limited conditions. Serine metabolism has often been shown to be reversible in other bacteria (24). But the flux through this pathway (PEP→serine) in MR-1 was much higher compared to the same pathway in *E. coli*, where the flux is 0.9-3.5% of total carbon utilization (43). High flux through serine metabolism suggested that MR-1 is able to oxidize excess C1. In C1 metabolism, one ATP and one NADPH are produced when serine is converted to formate via 5,10-Me-THF; an additional NADH is generated when the formate is completely oxidized to CO_2 (10). There are two additional pieces of evidence to support the serine oxidation route. First, high level of formate dehydrogenase (0.079 μmol/min/mg protein) has been reported for MR-1 under aerobic conditions (26). This enzyme is present in C1 oxidation route (Figure 4). Second, MR-1 can utilize glycine or serine as the sole carbon source

when grown in defined medium under aerobic condition (unpublished data). It would be advantageous for the cell to utilize the serine oxidation pathway to obtain energy (ATP, NADPH, and NADH). The same serine oxidation pathway has also been proposed in *Alteromonas putrefaciens* NCMB 1735 (21).

Under oxygen-limited conditions, the flux through the TCA cycle was reduced (<50%). Scott and Nealson proposed the existence of the serine pathway for MR-1 under anaerobic conditions (26). This view was established based on high levels of hydroxypyruvate reductase under anaerobic conditions. The fixation of carbon was postulated at the level of formaldehyde, which combines with glycine to yield serine (Figure 4). Under carbon-limited conditions, the labeling pattern of the α-carbon of serine is same as that of phenylalanine. This observation suggested that the α-carbon of serine was derived from the precursor, phospho*enol*pyruvate; however, under micro-aerobic conditions, the labeling pattern of the α-carbon of serine is different from that of phenylalanine and thus the calculated flux distribution showed another reversible route to produce glycine and serine (glyoxlate→glycine←→serine). This proposed pathway is consistent with the reported serine-glyoxylate aminotransferase activity when oxygen is limited (26, 27). However, no significant net flux through the serine pathway (serine → PEP → TCA cycle) was evident in oxygen-limited conditions based on the isotopomer model results.

The Pentose Phosphate, Entner-Doudoroff, Embden-Meyerhoff-Parnas, and Gluconeogenesis pathways

For *E. coli* grown on glucose, the PP pathway flux was over 20% of total carbon uptake and was utilized mainly for production of reducing equivalents (NADPH) and macromolecule precursors (43). Grown on lactate, the PP pathway flux of MR-1 was very low and only for biomass production. Comparing the two chemostat cultures, the average fluxes toward the ED

and PP pathways were higher under carbon-limited conditions than under oxygen-limited conditions, because more lactate was used for biomass production under carbon-limited conditions (no acetate production). The ED pathway flux was present in MR-1, consistent with the presence of the active ED pathway enzyme, 2-keto-3-deoxygluconate aldolase, under aerobic conditions (26). A few bacteria, including *Rhodobacter sphaeroides*, *Sinorhizobium meliloti*, and *Agrobacterium tumefaciens*, have been shown to substitute the ED pathway for the common EMP pathway (10, 19). These organisms usually lack two essential EMP enzymes, 6-phosphofructokinase and 1,6-biphosphofructoaldolase, which preclude them from using the EMP pathway. MR-1 does not contain phosphofructokinase but appears to contain 1,6-bisphosphofructo-aldolase and fructose-1,6-bisphosphatase (13, 26), which would allow it to synthesize glucose-6-phosphate using gluconeogenesis. As the Gibbs free energy of reaction suggests that the reaction of glucose-6-phosphate to 6-phosphogluconate is unidirectional (39), the reverse EMP pathway instead of the ED pathway is the only possible route to synthesize the carbohydrate precursor, glucose-6-phosphate.

Futile cycles

Two anapleurotic reactions appeared to be present (pyruvate to malate catalyzed by malate dehydrogenase and oxaloacetate to phospho*enol*pyruvate catalyzed by phospho*enol*pyruvate carboxykinase) and formed a futile cycle. In a previous study, malate dehydrogenase and phospho*enol*pyruvate carboxylase of MR-1 were shown to be active under aerobic conditions (26). In this study, the pyruvate-to-malate flux was around 13% of the lactate uptake under the carbon-limited condition and less than half this value under the oxygen-limited condition. A similar change in flux was also observed in the oxaloacetate to phospho*enol*pyruvate reaction under the two chemostat conditions.

Highly coupled to the anapleurotic reactions (via malate) is the glyoxylate shunt. The flux through the glyoxylate shunt was below 4% of the lactate uptake rate under both chemostat conditions. This finding correlated with the reported lower level (0.009 μmol/min/mg protein) of isocitrate lyase activity compared to other TCA cycle-related enzymes (26). The glyoxylate shunt is necessary for synthesizing TCA cycle intermediates, such as succinate and malate, and is also an important step for the serine pathway (isocitrate to glyoxylate to glycine) proposed for MR-1 under oxygen-limited conditions.

There appears to be a futile cycle involving the reactions pyruvate → malate, malate → oxaloacetate, and oxaloacetate → phospho*enol*pyruvate. It is not clear why the cell would choose to route flux through this circuitous pathway than directly through the reaction pyruvate → phospho*enol*pyruvate. These pathways might help to increase the flexibility in central carbon metabolism, to allow MR-1 to utilize different electron acceptors, or to maintain stability in central metabolism under environmental stresses (3, 34).

Flux ratios analysis and verification of model results

From GC-MS data (Table 3), the isotopomer distributions of key amino acids obtained from shake-flask cultures were relatively similar to those from chemostat cultures. However, based on the isotopomer data from the shake-flask cultures (using 3rd position labeled lactate), the fluxes through the TCA cycle and the reactions that transform acetyl-CoA to acetate were calculated to be 48% and 19% of lactate consumption, respectively. These values were very different from those obtained from either the carbon-limited or oxygen-limited chemostat cultures. As the shake-flask culture is non-steady state, the oxygen concentration changes from fully aerobic to micro-aerobic (31). It is known that the relative flux ratios rather than the absolute fluxes in key pathways determine the isotopomer distribution (23). The metabolic flux

ratios of key pathways were analyzed to reveal the similarity in the flux distribution of the central metabolism under the two chemostat and shake-flask conditions (Figure 5). Although acetate production, growth rate, and most intracellular fluxes were very different under these three conditions, many flux ratios in the TCA cycle and futile cycles did not vary significantly (the difference in the ratios between carbon-limited chemostat and shake-flask culture was below 5%). The same invariability in the flux ratios was also found in *Bacillus subtilis* and *E. coli* (7, 23). This observation suggests that central metabolism in some microorganisms is under specific regulation and is robust to environmental changes (28). Even though the shake-flask culture conditions were not identical to those of the chemostat cultures, the robust nature of bacterial metabolism helps maintain its relative flux ratios. This supports the idea that shake-flask cultures may sometimes substitute for continuous culture for metabolic flux analysis, at least to obtain a reliable measurement of central metabolic flux ratios (23).

As our study showed that the isotopomer distributions in *S. oneidensis* MR-1 were not sensitive to culture methods in the aerobic condition, the isotopomer distribution from shake flasks with different labeled lactate substrates is an efficient and reliable approach to check the accuracy of the flux estimations from chemostat cultures. First, using 99% [1-^{13}C] L-lactate as the carbon source, the model used the flux distribution from the carbon-limited conditions to predict the isotopomer distribution of six key amino acids. The model prediction was then compared with the experimental isotopomer distribution obtained from the culture grown aerobically in shake flasks containing 30 mM 99% [1-^{13}C] L-lactate. The accuracy of the flux estimation was validated since the experimental isotopomer data was consistent with the model predictions (Table 6).

GC-MS and NMR measurements of isotopomer distributions in proteinogenic amino acids, the annotated genome, and mathematical algorithms enabled us to develop a metabolic pathway model to quantify the intracellular fluxes of the central metabolic pathways. The results revealed a general metabolic flux distribution under both carbon-limited and oxygen-limited conditions. Our study also identified several active pathways, including a potential futile cycle, the ED pathway, the serine oxidation pathway, and activity of serine-glyoxylate aminotransferase (micro-aerobic condition). Furthermore, this research demonstrates successful applications of NMR and GC-MS for metabolic flux analysis, particularly where low fractions of fully labeled substrates were used.

Acknowledgements

We thank Drs. Jim Fredrickson, Yuri Gorby, and Grigoriy Pinchuk (Pacific Northwest National Laboratory, Richland, WA) for advice on culturing MR-1. We also thank Adam Meadows, Farnaz Nowroozi, Kenny Tran, and Kishen Guna (University of California, Berkeley) for helping with experiments and isotopomer modeling. This work is part of the Virtual Institue for Microbial Stress and Survival (http://VIMSS.lbl.gov) supported by the U.S. Department of Energy, Office of Science, Office of Biological and Environmental Research, Genomics:GTL Program through contract DE-AC02-05CH11231 between the Lawrence Berkeley National Laboratory and the US Department of Energy.

References

1. **Alm, E. J., K. H. Huang, M. N. Price, R. P. Koche, K. Keller, I. L. Dubchak, and A. P. Arkin.** 2005. The MicrobesOnline Web site for comparative genomics. Genome Res. **15:**1015-1022.
2. **Arauzo-Bravo, M. J., and K. Shimizu.** 2003. An improved method for statistical analysis of metabolic flux analysis using isotopomer mapping matrices with analytical expressions. Journal of Biotechnology **105:**117-133.
3. **Christiansen, T., B. Christensen, and J. Nielsen.** 2002. Metabolic network analysis of *Bacillus claussi* on minimal and semirich medium using ^{13}C-Labeled glucose. Metabolic Engineering**:**159-169.
4. **Daniels, L., R. S. Hanson, and et al.** 1994. Chemical Analysis, p. 512-554. *In* P. Gerhardt, R. Murray, W. Wood, and N. Krieff (ed.), Method for General and Molecular Bacteriology. American Society of Microbiology, Washington DC.
5. **Delaglio, F., S. Grzesiek, G. Vuister, G. Zhu, J. Pfeifer, and A. Bax.** 1995. NMR pipe: a multidimensional spectral processing system based on UNIX pipes. Journal of Biomolecular NMR **6:**277-293.
6. **Dookeran, N. N., T. Yalcin, and A. G. Harrison.** 1996. Fragmentation reactions of protonated α-amino acids. Journal of Mass Spectrometry **31:**500-508.
7. **Fischer, E., and U. Sauer.** 2005. Large-scale *in vivo* flux analysis shows rigidity and suboptimal performance of *Bacillus subtilis* metabolism. Nature Genetics **37:**636-640.
8. **Fischer, E., and U. Sauer.** 2003. Metabolic flux profiling of *Escherichia coli* mutants in central carbon metabolism using GC-MS. Euro. J. Biochem **270:**880-891.
9. **Fischer, E., N. Zamboni, and U. Sauer.** 2004. High-throughput metabolic flux analysis based on gas chromatography-mass spectrometry derived 13C constraints. Analytical Biochemistry **325:**308-316.
10. **Fuhrer, T., E. Fischer, and U. Sauer.** 2005. Experimental identification and quantification of glucose metabolism in seven bacterial species. Journal of Bacteriology **187:**1581-1590.
11. **Ghosal, D., M. Omelchenko, E. Gaidamakova, V. Matrosova, A. Vasilenko, A. Venkateswaran, M. Zhai, H. Kostandarithes, H. Brim, K. Makarova, L. Wackett, J. Fredrickson, and M. Daly.** 2005. How radiation kills cells: survival of Deinococcus radiodurans and Shewanella oneidensis under oxidative stress. FEMS Microbiology Reviews **29:**361-375.
12. **Harrison, A. G.** 2001. Ion chemistry of protonated glutamic acid derivatives. International Journal of Mass Spectrometry **210/211:**361-370.
13. **Heidelberg, J. F., I. T. Paulsen, I. T. Nelson, E. J. Gaidos, W. C. Nelson, T. D. Read, J. A. Eisen, R. Seshadri, N. Ward, B. Methe, R. A. Clayton, T. Meyer, A. Tsapin, J. Scott, M. Beanan, L. Brinkac, S. Daugherty, R. T. DeBoy, R. J. Dodson, A. S. Durkin, D. H. Haft, J. F. Kolonay, R. Madupu, J. D. Peterson, L. A. Umayam, O. White, A. M. Wolf, J. Vamathevan, J. Weidman, M. Impraim, K. Lee, K. Berry, C. Lee, J. Mueller, H. Khouri, J. Gill, T. R. Utterback, L. A. McDonald, T. V. Feldblyum, H. O. Smith, J. C. Venter, K. H. Nealson, and C. M. Fraser.** 2002. Genome sequence of the dissimilatory metal-ion reducing bacterium Shewanella oneidensis. Nature Biotechnology **20:**1118-1123.

14. **Hellerstein, M. K., and R. A. Neese.** 1999. Mass isotopomer distribution analysis at eight years: theoretical, analytic, and experimental considerations. American Journal of Physiology-Endocrinology and Metabolism **276:**E1146-E1170.
15. **Herbert, D., P. J. Phipps, and e. al.** 1971. Chemical Analysis of Microbial Cells, p. 210-344. *In* J. R. Norris and D. W. Ribbons (ed.), Methods in Microbiology, vol. 5B. Academic Press, Inc., New York.
16. **Marshal, J.** 2004. Production of secondary metabolites from acetyl Co-A precursors in bacterial and fungal hosts. PhD thesis. University of California, Berkeley.
17. **Middleton, S. S., R. B. Latmani, M. R. Mackey, M. H. Ellisman, B. M. Tebo, and C. S. Criddle.** 2003. Cometabolism of Cr(VI) by *Shewanella oneidensis* MR-1 producess cell-associated reduced chromium and inhibits growth. Biotechnology and Bioengineering **83:**627-637.
18. **Neal, A. L., K. Lowe, T. L. Daulton, J. Jones-Meehan, and B. J. Little.** 2002. Oxidation state of chromium associated with cell surfaces of *shewanella oneidensis* during chromate reduction. Applied Surface Science **202:**150-159.
19. **Nicklin, J., K. Graeme-Cook, T. Paget, and R. A. Killington.** 1999. Instant Notes in Microbiology. Bios Scientific Publishers, London, UK.
20. **Press, W. H., S. A. Teukolsky, W. T. Vetterling, and B. P. Flannery.** 1992. Numerical Recipes in FORTRAN, 2nd ed. Cambridge University Press, Cambridge.
21. **Ringo, E. E., E. Stenberg, and A. R. Strom.** 1984. Amino acid and lactate catabolism in trimethylamine oxide respiration of *Alteromonas putrefaciens* NCMB 1735. Applied and Environmental Microbiology **47:**1084-1089.
22. **Sauer, U.** 2004. High-throughput phenomics: experimental methods for mapping fluxomes. Current Opinion in Biotechnology **15:**58-63.
23. **Sauer, U., D. R. Lasko, J. Fiaux, M. Hochuli, R. Glaser, T. Szyperski, K. Wuthrich, and J. E. Bailey.** 1999. Metabolic flux ratio analysis of genetic and environmental modulations of Escherichia coli central carbon metabolism. Journal of Bacteriology **181:**6679-6688.
24. **Schmidt, K., J. Nielsen, and J. Villadsen.** 1999. Quantitative analysis of metabolic fluxes in *Escherichia coli*, using two-dimensional NMR spectroscopy and complete isotopomer models. Journal of Biotechnology **71:**175-190.
25. **Schmidt, K., L. C. Norregaard, B. Pedersen, A. Meissner, and J. Q. Nielsen.** 1999. Quantification of intracellular metabolic fluxes from fractional enrichment and ^{13}C-^{13}C coupling constraints on the isotopomer distribution in labeled biomass components. Metabolic Engineering **1:**166-179.
26. **Scott, J. H., and K. H. Nealson.** 1994. A Biochemical Study of the Intermediary Carbon Metabolism of Shewanella putrefaciens. Journal of Bacteriology **176:**3408-3411.
27. **Serres, M. H., and M. Riley.** 2006. Genomic Analysis of Carbon Source Metabolism of *Shewanella oneidensis* MR-1: Predictions versus Experiments. Journal of Bacteriology **188:**4601-4609.
28. **Stelling, J., U. Sauer, Z. Szallasi, F. Doyle, and J. Doyle.** 2004. Robustness of cellular functions. Cell **118:**675-685.
29. **Stephanopoulos, G. N., A. A. Aristidou, and J. Nielsen.** 1998. Metabolic Engineering Principles and Methodologies. Academic Press, San Diego.

30. **Szyperski, T.** 1995. Biosynthetically directed fractional ^{13}C labeling of proteinogenic amino acids: an efficient analytical too to investigate intermediary metabolism. Euro J Biochem **232:**433-448.
31. **Tang, Y. J., D. Laidlaw, K. Gani, and J. D. Keasling.** 2006. Evaluation of the effects of various culture conditions on Cr(VI) reduction by *Shewanella oneidensis* MR-1 in a novel high-throughput mini-bioreactor. Biotechnology and Bioengineering **95:**176-184.
32. **Tang, Y. J., A. L. Meadows, and J. D. Keasling.** 2006. A kinetic model describing *Shewanella oneidensis* MR-1 growth, substrate consumption, and product secretion. Biotechnology and Bioengineering **In press**.
33. **Teece, M. A., M. L. Fogel, M. E. Dollhopf, and K. H. Nealson.** 1999. Iostopic fraction associated with biosynthesis of fatty acids by a marine bacterium under oxic and anoxic conditions. Organic Geochemistry **30:**1571-1579.
34. **Tiedje, J.** 2002. Shewanella- the environmentally versatile genome. Nature Biotechnology **20:**1093-1094.
35. **Venkateswaran, K., D. P. Moser, M. E. Dollhopf, D. P. Lies, D. A. Saffarini, B. J. MacGregor, D. B. Ringelberg, D. C. White, M. Nishijima, H. Sano, J. Burghardt, E. Stackebrandt, and K. H. Nealson.** 1999. Polyphasic taxonomy of the genus *Shewanella* and description of *Shewanella oneidensis sp*. International Journal of Systematic Bacteriology **49:**705-724.
36. **Viamajala, S., B. M. Peyton, W. A. Apel, and J. N. Petersen.** 2002. Chromate/nitrite interactions in *Shewanella oneidensis* MR-1: Evidence for multiple hexavalent chromium [Cr(VI)] reduction mechanisms dependent on physiological growth conditions. Biotechnology and bioengineering **78:**770-778.
37. **Viamajala, S., B. M. Peyton, R. K. Sani, W. A. Apel, and J. N. Petersen.** 2004. Toxic effect of chromium(VI) on anaerobic and aerobic growth of *Shewanella oneidensis* MR-1. Biotechnology Progress **20:**87-95.
38. **Wiechert, W.** 2001. ^{13}C Metabolic Flux Analysis. Metabolic Engineering **3:**195-206.
39. **Wiechert, W., and A. A. de Graaf.** 1997. Bidirectional reaction steps in metabolic networks I. Modeling and simulation of carbon isotope labeling experiments. Biotechnology and Bioengineering **55:**101-117.
40. **Wiechert, W., M. Mollney, S. Petersen, and A. A. de Graaf.** 2001. A universal framework for ^{13}C metabolic flux analysis. Metabolic Engineering **3:**265-283.
41. **Wiechert, W., C. Siefke, A. A. de Graaf, and A. Marx.** 1997. Bidirectional reaction steps in metabolic networks: II. Flux estimation and statistical analysis. Biotechnology and Bioengineering **55:**118-135.
42. **Zhang, C. L., Y. Li, Q. Ye, J. Fong, A. D. Peacock, E. Blunt, J. Fang, D. R. Lovley, and D. C. White.** 2003. Carbon isotope signatures of fatty acids in *Geobacter metallireducens* and *Shewanella algae*. Chemical Geology **195:**17-28.
43. **Zhao, J., and K. Shimizu.** 2003. Metabolic flux analysis of Escherichia coli K12 grown on 13C-labeled acetate and glucose using GC-MS and powerful flux calculation method. Journal of Biotechnology **101:**101-117.

Figures Captions

Figure 1. Pathways of lactate metabolism in *S. oneidensis* MR-1. The shaded boxes represent biomass. The dashed arrow (reaction 21e) is not present in the annotated genome sequence. The amino acids used for isotopomer models are in parenthesis. Numbers represent the reactions included in the model (corresponding to the reactions listed in the Supplementary Material). Abbreviations: 6PG, 6-phosphogluconate; ACoA, acetyl-coenzyme A; C1, 5,10-Me-THF; C5P, ribose-5-phosphate (or ribulose-5-phosphate or xylulose-5-phosphate); CIT, citrate; E4P, erythrose-4-phosphate; F6P, fructose-6-phosphate; G6P, glucose-6-phosphate; ICT, isocitrate; MAL, malate; OAA, oxaloacetate; OXO, 2-oxoglutarate; PEP, phosphoenolpyruvate; PGA, 3-phosphoglycerate; PYR, pyruvate. S7P, sedoheptulose-7-phosphate; SUC, succinate; T3P, triose-3-phosphate;

Figure 2. Time courses of biomass growth (♦), lactate concentration (■), and acetate secretion (▲) in chemostat experiments under carbon-limited conditions (A) and oxygen-limited conditions (B). All data points have error bars representing the errors in the measurement; some error bars are not visible due to the very small measurement errors.

Figure 3. (A) *In vivo* flux distribution in the central metabolism of *S. oneidensis* MR-1 under carbon-limited (upper number), shake-flask (middle number, in parentheses), and oxygen-limited (lower number) conditions. The abbreviations are the same as used in Figure 1. (B) The exchange coefficients for significant reversible fluxes estimated in carbon-limited (upper number) and oxygen-limited (lower number) chemostat cultures.

Figure 4. The proposed serine pathway under anaerobic conditions is shown by the solid arrows. The direction of the serine oxidation pathway under aerobic conditions is shown by the dashed arrows.

Figure 5. Relative flux ratios in the central metabolic pathways under carbon-limited chemostat, oxygen-limited chemostat, and shake-flask cultures. The flux ratio represents the relative relationships between key metabolic routes. Acetate production, v6/v1; serine-glyoxylate aminotransferase, v21e/v12; malate synthase/TCA, v8/v14; serine metabolism/glycolysis, (v21+v21e)/v3; glyoxylate shunt/TCA, v15/v10; phospho*enol*pyruvate synthase/TCA, v4/v14; ED pathway/glycolysis, v28/v22. Empty bars, oxygen-limited; stippled bars, carbon-limited; filled bars, shake flasks.

Figures

Figure 1

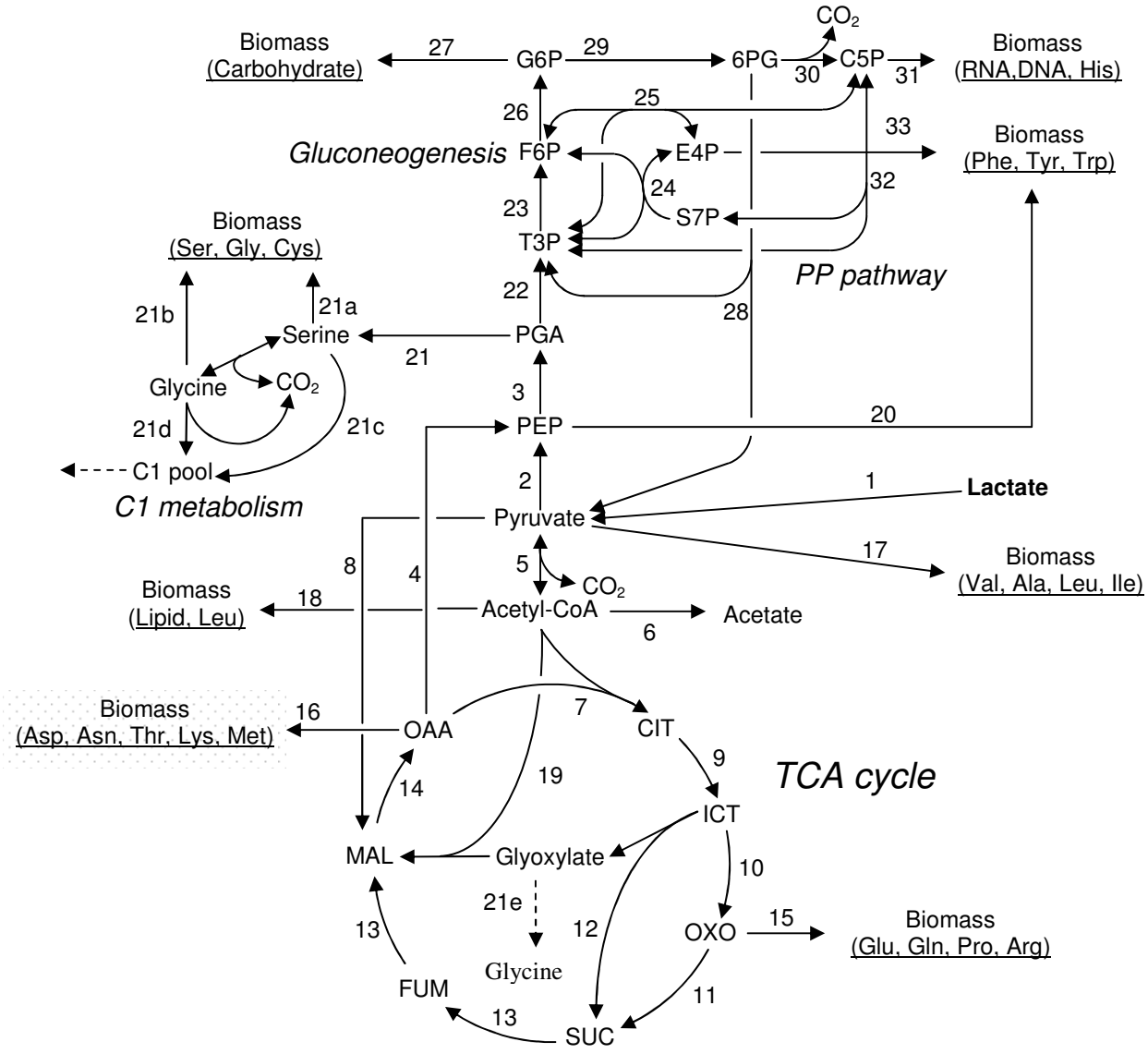

Figure 2

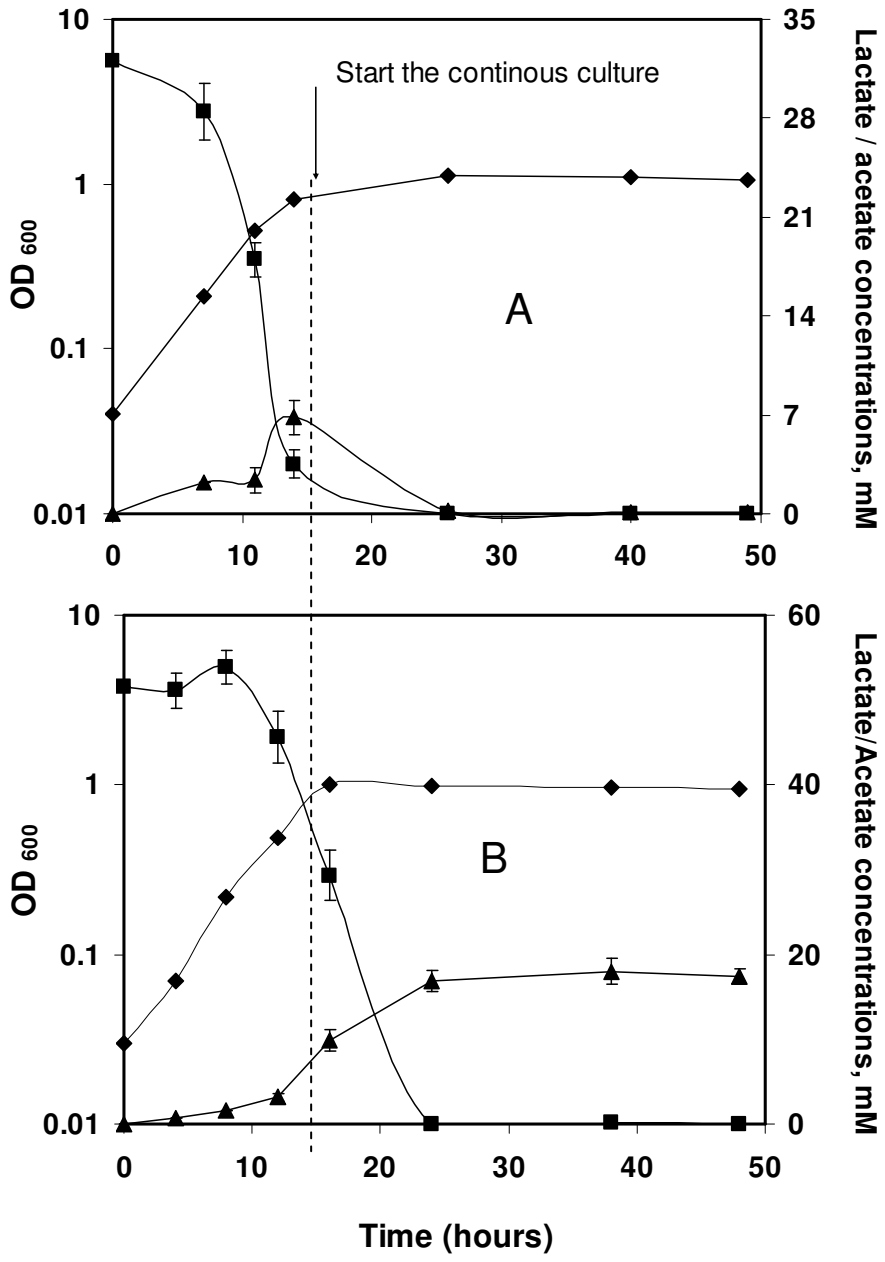
Start the continous culture
A
B
OD 600
Lactate / acetate concentrations, mM
Lactate/Acetate concentrations, mM
Time (hours)
10
1
0.1
0.01
35
28
21
14
7
0
60
40
20
0
0
10
20
30
40
50

Figure 3

A

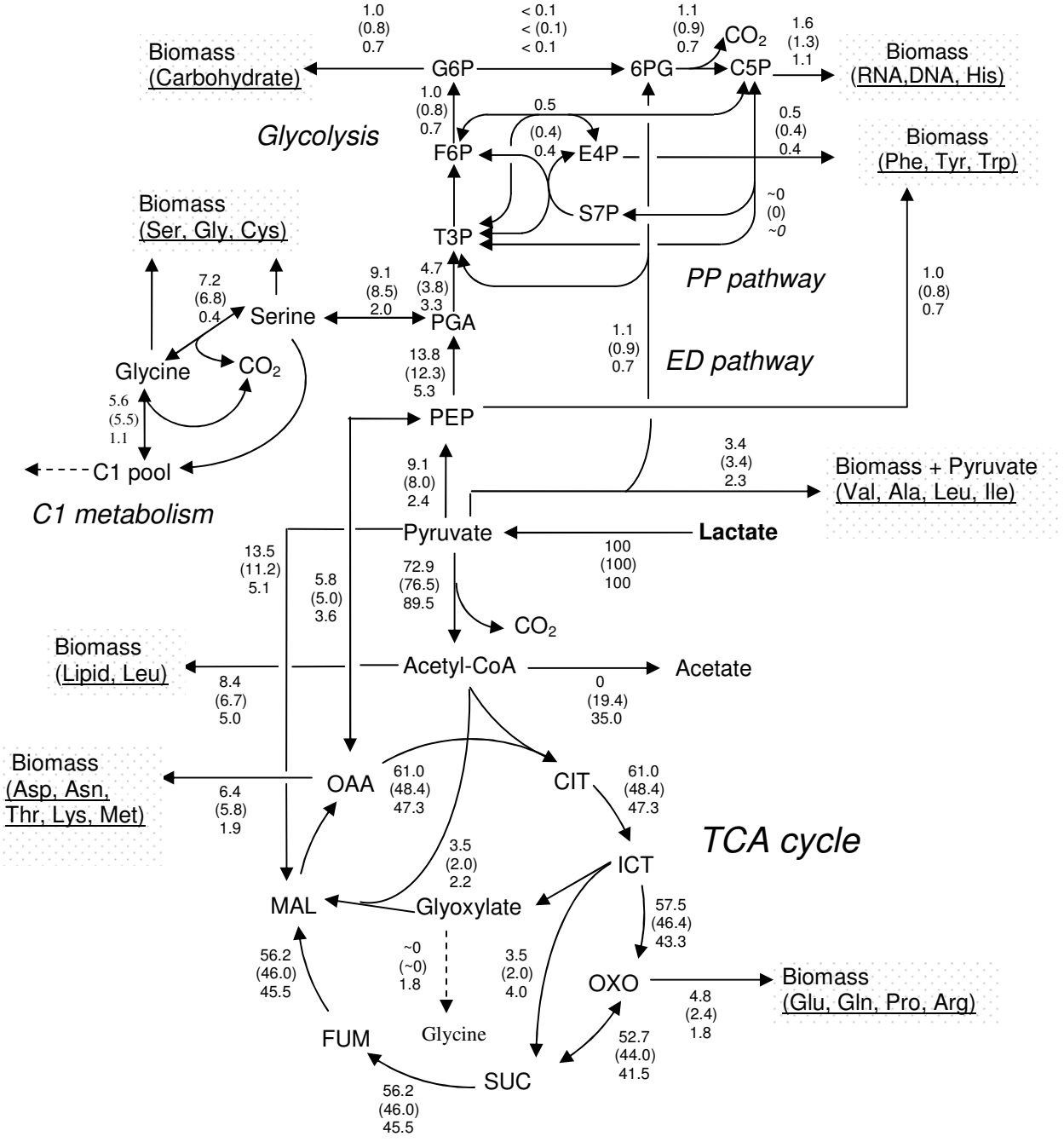
Biomass (Carbohydrate)
G6P
6PG
C5P
CO2
Biomass (RNA,DNA, His)
Glycolysis
F6P
E4P
Biomass (Phe, Tyr, Trp)
S7P
T3P
Biomass (Ser, Gly, Cys)
PP pathway
Serine
PGA
Glycine
CO2
ED pathway
PEP
C1 pool
C1 metabolism
Biomass + Pyruvate (Val, Ala, Leu, Ile)
Pyruvate
Lactate
CO2
Biomass (Lipid, Leu)
Acetyl-CoA
Acetate
Biomass (Asp, Asn, Thr, Lys, Met)
OAA
CIT
TCA cycle
ICT
MAL
Glyoxylate
OXO
Biomass (Glu, Gln, Pro, Arg)
FUM
Glycine
SUC

B


0.20
0.45
C1
0.60
0.95
Gly
0.25
0.35
Ser
PGA
0.10
0.40
OAA
PEP
0.85
0.85
SUC
OXO

Figure 4

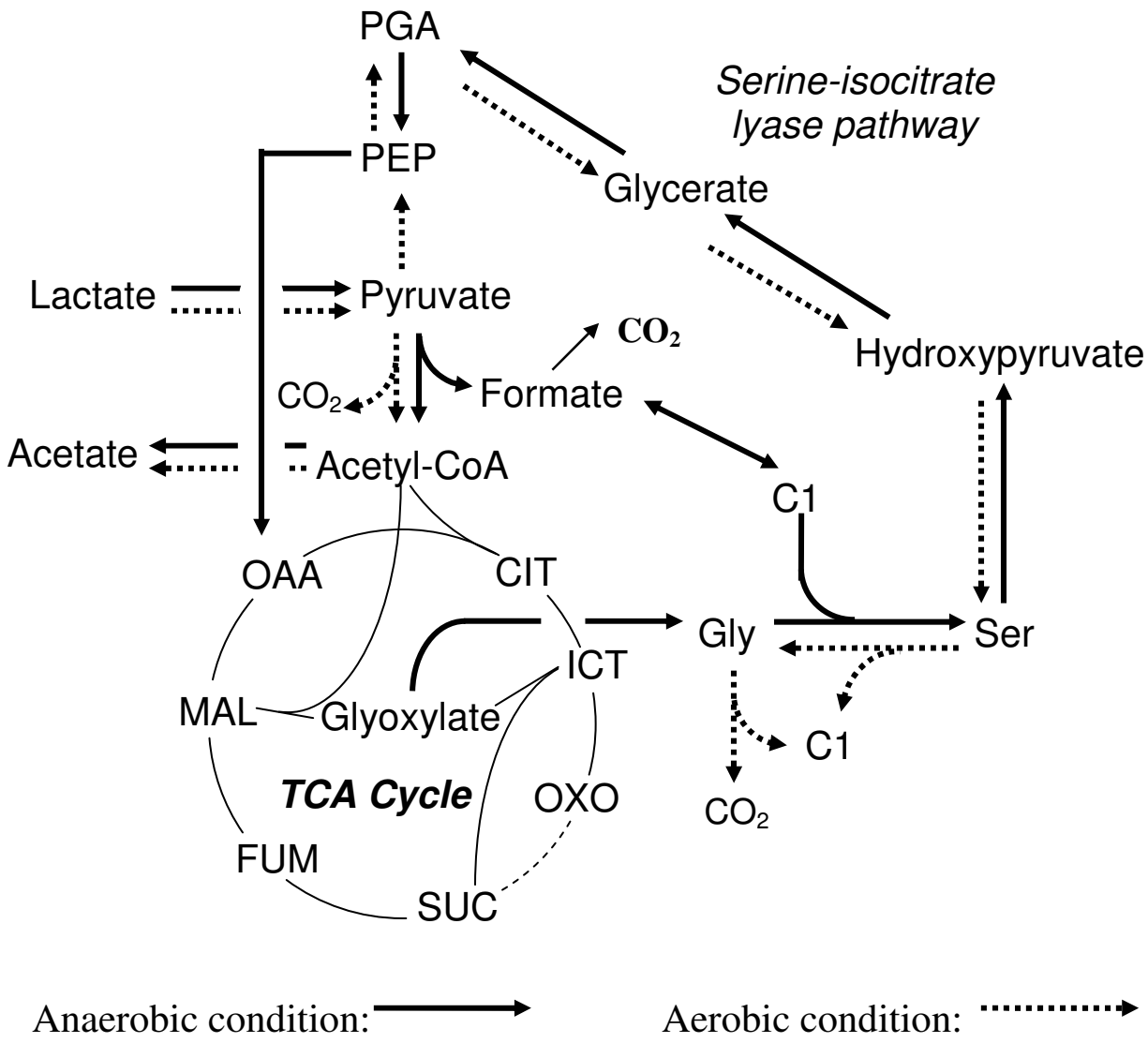
PGA
PEP
Serine-isocitrate
lyase pathway
Glycerate
Lactate
Pyruvate
CO2
Hydroxypyruvate
CO2
Formate
Acetate
Acetyl-CoA
C1
OAA
CIT
Gly
Ser
ICT
MAL
Glyoxylate
C1
TCA Cycle
OXO
CO2
FUM
SUC
Anaerobic condition:
Aerobic condition:

Figure 5

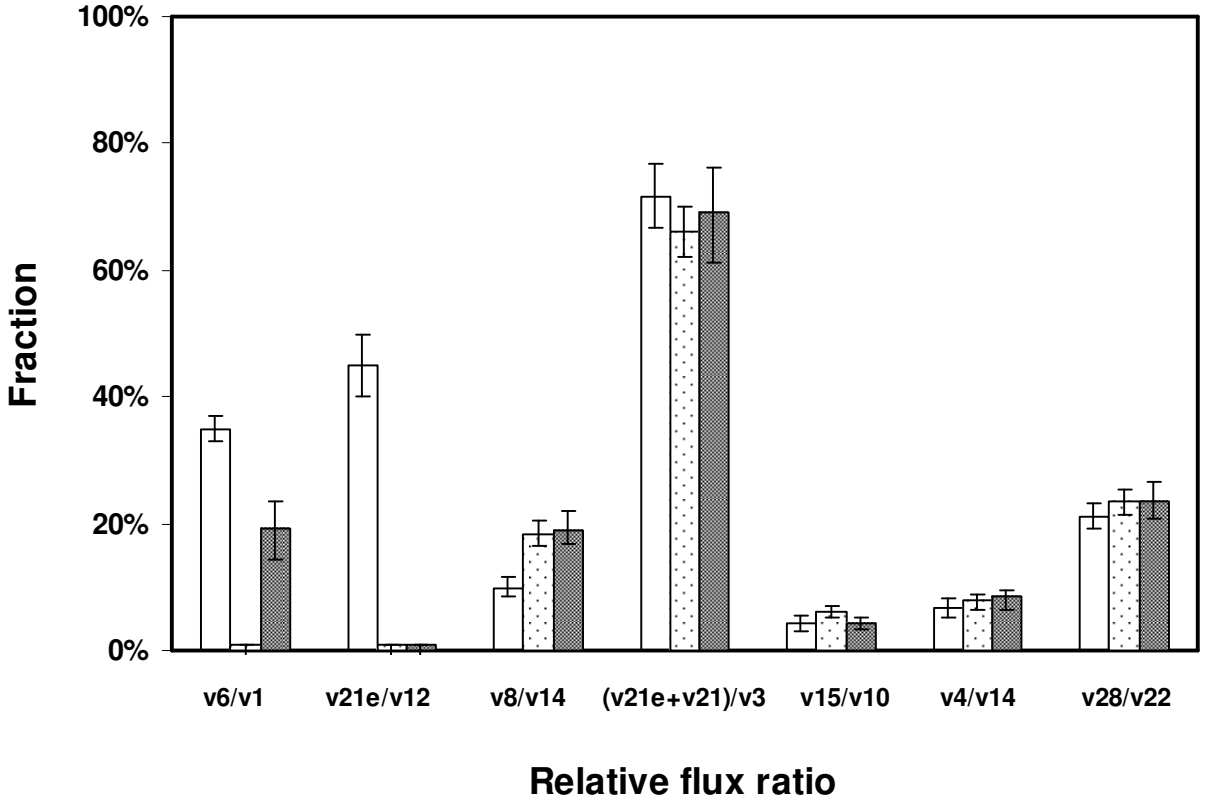
100%
80%
60%
40%
20%
0%
Fraction
v6/v1
v21e/v12
v8/v14
(v21e+v21)/v3
v15/v10
v4/v14
v28/v22
Relative flux ratio

Tables

Table 1. Comparison of cultivation parameters of *S. oneidensis* MR-1 cultures.

Cultivation conditions	Shake flasks, n=5	Chemostat, oxygen-limited	Chemostat, carbon-limited
Growth or dilution rate (hr^{-1})	0.17	0.10	0.079
Sampling OD_{600}	~0.5	~1.0	~1.0
Dissolved oxygen level	ND*	>70%	0~10%
Biomass concentration (g/L)	0.26±0.04	0.63 ± 0.05	0.58 ± 0.03
Lactate remained (mM)	13.5 ± 1.1	~0.3	~0
Acetate excreted (mM)	3.2 ± 0.6	17.5 ± 0.9	~0
Pyruvate excreted (mM)	~0.5	~0.1	~0
Lactate consumption rate (mM/g DCW h)	7.2 ± 0.7	7.9 ± 0.6	4.1 ± 0.3
CO_2 formation rate (mM/g DCW h)	ND	13.7 ± 1.5	9.8 ± 1.2

*ND, not determined. Dissolved oxygen dropped during the exponential growth phase in shake flasks (31).

Table 2. Comparison in biomass composition between *S. oneidensis* MR-1 and *E. coli*.

	S. oneidensis MR-1			*E. coli*
Cultivation conditions	Shake flask[a]	Chemostat, oxygen-limited	Chemostat, carbon-limited	Reported value[b]
Protein (%)	51 ± 5	48 ± 3	48 ± 4	52
RNA (%)	16.2 ± 1.9	14.0 ± 2.5	13.6 ± 2.3	16
DNA (%)	2.7 ± 0.4	2.5 ± 0.4	2.1 ± 0.5	3
Fatty acids (%)	9.2 ± 1.2	15.1 ± 1.2	14.8 ± 0.8	9.1 (lipid fraction)
Carbohydrate (%)	12 ± 2	11 ± 3	10 ± 3	17
Others (%)	~8.9	~9.4	~9.5	3 (ash weight)

[a]30mM lactate was used.
[b]Glucose medium under aerobic culture, values adapted from Stephanopoulos, et al. (1998).

Table 3. Measured and predicted (in parenthesis) mass fragment $[M-57]^+$ distribution of TBDMS-derivatized amino acids from *S. oneidensis* MR-1 hydrolysates*.

Amino Acid	**Ions**	**Chemostat, carbon-limited**	**Shake flask, 3-^{13}C** [1]	**Chemostat, oxygen-limited**	**Shake flask, 10% $^{13}C_3$** [2]
Ala	M0	0.01 (0.02)	0.02 ± 0.01	0.90 (0.89)	0.89 ± 0.01
	M1	0.98 (0.97)	0.97 ± 0.01	0 (0.01)	0 ± 0
	M2	0 (0.01)	0.0 ± 0	0.01 (0)	0.01 ± 0
Val	M0	0.01 (0.01)	0 ± 0	0.79 (0.81)	0.81 ± 0
	M1	0.03 (0.02)	0.02 ± 0.01	0.01 (0.01)	0.01 ± 0
	M2	0.92 (0.95)	0.92 ± 0.02	0.10 (0.09)	0.10 ± 0.01
	M3	0.01 (0.01)	0.01 ± 0.01	0.09 (0.09)	0.08 ± 0
Asp/Asn	M0	0 (0)	0 ± 0	0.75 (0.76)	0.77 ± 0.02
	M1	0.20 (0.18)	0.20 ± 0.02	0.15 (0.13)	0.13 ± 0.02
	M2	0.40 (0.40)	0.39 ± 0.01	0.07 (0.09)	0.05 ± 0.02
	M3	0.40 (0.41)	0.41 ± 0.02	0.03 (0.02)	0.06 ± 0.02
Met	M0	0.01 (0)	0.01 ± 0	0.64 (0.65)	0.66 ± 0.03
	M1	0.04 (0.05)	0.05 ± 0.01	0.21 (0.21)	0.22 ± 0.02
	M2	0.22 (0.24)	0.24 ± 0.02	0.12 (0.10)	0.09 ± 0.02
	M3	0.39 (0.40)	0.38 ± 0.03	0.03 (0.04)	0.03 ± 0.01
Ser	M0	0.07 (0.06)	0.06 ± 0.02	0.86 (0.87)	0.85 ± 0
	M1	0.72 (0.72)	0.74 ± 0.03	0.07 (0.04)	0.06 ± 0.01
	M2	0.16 (0.16)	0.15 ± 0.02	0.03 (0.02)	0.03 ± 0
Gly	M0	0.68 (0.69)	0.69 ± 0.02	0.88 (0.87)	0.90 ± 0.01
	M1	0.21 (0.23)	0.22 ± 0.02	0.04 (0.06)	0.01 ± 0

Glu/Gln	M0	0 (0)	0 ± 0	0.70 (0.71)	0.72 ± 0.03
	M1	0.01 (0.01)	0.01 ± 0	0.15 (0.14)	0.14 ± 0.01
	M2	0.31 (0.30)	0.32 ± 0.02	0.12 (0.13)	0.12 ± 0
	M3	0.48 (0.49)	0.48 ± 0.01	0.02 (0.02)	0.02 ± 0
	M4	0.18 (0.19)	0.20 ± 0.01	0 (0)	0 ± 0
Phe	M0	0 (0)	0 ± 0	0.57 (0.55)	0.61 ± 0.05
	M1	0 (0)	0 ± 0	0.17 (0.18)	0.12 ± 0.03
	M2	0.02 (0.03)	0.01 ± 0.01	0.09 (0.10)	0.08 ± 0.02
	M3	0.45 (0.38)	0.61 ± 0.11	0.12 (0.12)	0.14 ± 0.04
	M4	0.30 (0.32)	0.19 ± 0.06	0.03 (0.03)	0.02 ± 0.01
	M5	0.14 (0.18)	0.09 ± 0.03	0.01 (0.01)	0.02 ± 0.01
His	M0	0.01 (0)	0 ± 0	0.71 (0.68)	0.73 ± 0.03
	M1	0.04 (0.03)	0.05 ± 0.01	0.07 (0.13)	0.04 ± 0.03
	M2	0.26 (0.27)	0.27 ± 0.02	0.11 (0.10)	0.11 ± 0
	M3	0.50 (0.50)	0.49 ± 0.02	0.09 (0.08)	0.11 ± 0.01
	M4	0.11 (0.14)	0.06 ± 0.03	0.01 (0.01)	0 ± 0
$^{13}CO_2$ percentage in total CO_2 (based on the off gas composition)					
$\frac{^{13}CO_2}{CO_2}$		0.13 (0.14)[3]	ND	0.04 (0.03)[3]	ND

* Mass distributions of tyrosine and threonine were identical to phenylalanine and aspartate, respectively.

[1] Shake-flask culture at exponential phase with 98% [3-^{13}C] L-lactate (30mM), standard deviation of isotopomer data were based on three replicates.

[2] Shake-flask culture at exponential phase with a mixture of 10% fully-labeled L-lactate and 90% unlabeled lactate (30mM), n=3.

[3] $^{13}CO_2$ fraction is based on off-gas composition.

Table 4. NMR measurement and model prediction (in parenthesis) ^{13}C isotopomer distribution of key amino acids from *S. oneidensis* MR-1 hydrolysates.

Amino Acid	α-carbon fragments	Chemostat, carbon-limited[1]	Chemostat, oxygen-limited [1]
α-Asp	Cα	0.23 (0.18)	0.37 (0.33)
	Cα-Cβ	0.47 (0.49)	0.11 (0.06)
	Cα-C=O	0.05 (0.02)	0.42 (0.47)
	Cβ-Cα-C=O	0.25 (0.30)	0.10 (0.13)
α-Ser	Cα	0.17 (0.17)	0.21 (0.19)
	Cα-Cβ	0.52 (0.51)	0.06 (0.03)
	Cα-C=O	0.07 (0.02)	0.26 (0.28)
	Cβ-Cα-C=O	0.25 (0.29)	0.47 (0.50)
α-Gly	Cα	0.70 (0.68)	0.41 (0.41)
	Cα-C=O	0.29 (0.32)	0.59 (0.59)
α-Glu	Cα	0.25 (0.32)	0.31 (0.32)
	Cα-Cβ	0.45 (0.43)	0.15 (0.13)
	Cα-C=O	0.06 (0.04)	0.54 (0.51)
	Cβ-Cα-C=O	0.24 (0.22)	0.01 (0.04)
α-Phe	Cα	0.18 (0.17)	0.14 (0.10)
	Cα-Cβ	0.51 (0.51)	0.01 (0.01)
	Cα-C=O	0.04 (0.02)	0.04 (0.11)
	Cβ-Cα-C=O	0.27 (0.29)	0.83 (0.77)
β-Ser	Cβ	0.81 (0.82)	0.50 (0.49)
	Cβ-Cα	0.19 (0.18)	0.50 (0.51)
β-Asp	Cβ	0.26 (0.32)	0.36 (0.33)
	Cβ-Cα	0.41 (0.41)	0.15 (0.13)
	Cβ-Cγ	0.07 (0.04)	0.40 (0.47)
	Cα-Cβ-Cγ	0.26 (0.23)	0.09 (0.07)
β-Glu	Cβ	0 (0)	0.72 (0.73)
	Cβ-Cα or Cβ-Cγ	0.26 (0.21)	0.28 (0.27)
	Cα-Cβ-Cγ	0.73 (0.79)	0 (0.01)
β-Ala	Cβ	0.96 (0.98)	0.11 (0.10)
	Cβ-Cα	0.04 (0.02)	0.89 (0.90)
β-His	Cβ	NA[2]	0.10 (0.15)
	Cβ-Cα	NA[2]	0.90 (0.85)
	Cβ-Cγ	NA[2]	0 (0)
α-Ace	Cα	ND[3]	0.11 (0.10)
	Cα-Cβ	ND[3]	0.89 (0.90)

[1] The standard deviation for NMR measurement was 4-5%.
[2] NA, natural abundance.
[3] ND, not determined.

Table 5. Sensitivity test of predicted mass distribution signals (GC-MS $[M-57]^+$ and NMR [α or β carbon]) for aspartate and glutamate upon changes in the futile flux, v8.

	GC-MS Data			NMR Data		
Amino acids	Sensitivity coefficient	3rd carbon labeled [1]	Fully labeled [2]	Sensitivity coefficient	3rd carbon labeled [1]	Fully labeled [2]
	$\left\|\frac{\Delta M_0}{\Delta v_8}\right\|$	0.0001	0.0041	$\left\|\frac{\Delta C\alpha}{\Delta v_8}\right\|$	0.013	0.015
Asp	$\left\|\frac{\Delta M_1}{\Delta v_8}\right\|$	0.0100	0.0057	$\left\|\frac{\Delta C\alpha - C\beta}{\Delta v_8}\right\|$	0.005	0.008
	$\left\|\frac{\Delta M_2}{\Delta v_8}\right\|$	0.0089	0.0001	$\left\|\frac{\Delta C\alpha - C=O}{\Delta v_8}\right\|$	~0	0.002
	$\left\|\frac{\Delta M_3}{\Delta v_8}\right\|$	0.0179	0.0011	$\left\|\frac{\Delta C\beta}{\Delta v_8}\right\|$	0.016	0.019
	$\left\|\frac{\Delta M_0}{\Delta v_8}\right\|$	~0	0.0024	$\left\|\frac{\Delta C\alpha}{\Delta v_8}\right\|$	0.019	0.018
	$\left\|\frac{\Delta M_1}{\Delta v_8}\right\|$	0.0006	0.0039	$\left\|\frac{\Delta C\alpha - C\beta}{\Delta v_8}\right\|$	0.012	0.016
Glu	$\left\|\frac{\Delta M_2}{\Delta v_8}\right\|$	0.0132	0.0016	$\left\|\frac{\Delta C\alpha - C=O}{\Delta v_8}\right\|$	~0	0.003
	$\left\|\frac{\Delta M_3}{\Delta v_8}\right\|$	0.0053	0.0003	$\left\|\frac{\Delta C\beta - C\alpha - C=O}{\Delta v_8}\right\|$	0.006	0.003
	$\left\|\frac{\Delta M_4}{\Delta v_8}\right\|$	0.0082	0.0001	$\left\|\frac{\Delta C\beta}{\Delta v_8}\right\|$	~0	0.016
Sum of squares		0.00077	0.00007		0.00082	0.00128

[1] Data from the carbon-limited chemostat

[2] Data from the oxygen-limited chemostat

Table 6. Flux distribution reliability test: predicted and measured fragment mass $[M-57]^+$ distribution of key amino acids when [1-^{13}C] labeled lactate medium was used for shake-flask culture (n=2)*.

Related Pathway	Amino acids	Ion, m/z	Model prediction	Measured value
Pyruvate synthesis route	Ala	M0	0.02	0.03 ± 0.01
		M1	0.98	0.98 ± 0.01
		M2	0	0 ± 0
	Val	M0	0.02	0.05 ± 0.01
		M1	0.96	0.94 ± 0.01
		M2	0	0 ± 0
	Ser	M0	0.24	0.21 ± 0.03
		M1	0.76	0.79 ± 0.03
		M2	0.0	0 ± 0
Serine oxidation route	Gly	M0	0.25	0.34 ± 0.03
		M1	0.75	0.66 ± 0.03
		M2	0	0 ± 0
TCA cycle	Asp	M0	0.78	0.75 ± 0.04
		M1	0.12	0.14 ± 0.02
		M2	0.10	0.10 ± 0.01
	Glu/Gln	M0	0.89	0.86 ± 0.03
		M1	0.09	0.07 ± 0.02
		M2	0.01	0.03 ± 0.02
PP pathway	Phe	M0	0.01	0.01 ± 0
		M1	0.13	0.09 ± 0.03
		M2	0.42	0.36 ± 0.05
		M3	0.42	0.52 ± 0.08
	His	M0	0.23	0.18 ± 0.05
		M1	0.76	0.75 ± 0.06
		M2	0.01	0.04 ± 0.02

* The same flux rate distribution as listed in Figure 3 (the carbon-limited condition) was used for model prediction.